Block Polyelectrolyte Additives Modulate the Viscoelasticity and Enable 3D Printing of Gelatin Inks at Physiological Temperatures

Tobias Göckler,[1, 2, †] Defu Li, [1, †] Fahed Albreiki,[1, †] Alisa Grimm,[1, 2] Felix Mecklenburg,[2] Ute Schepers,[2, 3] Samanvaya Srivastava[1, 4, 5, *]

SUMMARY

We demonstrate the utility of block polyelectrolyte (bPE) additives to enhance viscosity and resolve longstanding challenges with the three-dimensional printability of extrusion-based biopolymer inks. The addition of oppositely charged bPEs into solutions of photocurable gelatin methacryloyl (GelMA) results in complexation-driven self-assembly of the bPEs, leading to GelMA/bPE inks that are printable at physiological temperatures, representing stark improvements over GelMA inks that suffer from low viscosity at 37 °C leading to low printability and poor structural stability. The hierarchical microstructure of the self-assemblies (either jammed micelles or three-dimensional networks) formed by the oppositely charged bPEs, as confirmed by small angle X-ray scattering, is attributed to the enhancements in the shear strength and printability of the GelMA/bPE inks. Varying bPE concentration in the inks is shown to enable tunability of the rheological properties to meet the criteria of pre- and post-extrusion flow characteristics for 3D bioprinting, including prominent yield stress behavior, strong shear thinning, and rapid recovery upon flow cessation. Moreover, the bPE self-assemblies also contribute to the robustness of the photocrosslinked hydrogels – photocrosslinked GelMA/bPE hydrogels are shown to exhibit higher shear strength than photocrosslinked GelMA hydrogels. We envision this study to serve as a practical guide for the bioprinting of bespoke extrusion inks where bPE are used as scaffolds and viscosity enhancers that can be emulated in a range of biopolymers and photocurable precursors.

PROGRESS AND POTENTIAL

Rapid prototyping using computer-aided 3D printing of cells is expected to revolutionize tissue engineering. However, efforts in biomaterials science and engineering to meet the growing needs of 'bioinks' for 3D bioprinting have remained hindered due to the poor mechanical properties of most bioinks during the deposition process. Extracellular matrix-derived materials, most famously gelatin-based materials, are archetypal examples that function very well as cell scaffoldings but are difficult to print at physiological temperatures. Here, by combining gelatin-based materials with block polymers containing charged and neutral segments, a novel hybrid ink is developed. The electrostatic self-assembly of the block polymers provides a scaffold augmenting the gelatin-based inks, enabling their printing at high resolutions. We anticipate the use of such inks to print complex organ-like constructs in the near term, opening avenues for their translation into medically relevant 3D bioprinting.

KEYWORDS: *Bioprinting, Tissue Engineering, Additive Manufacturing, Biofabrication, Polyelectrolyte Complexes, Self-Assembly*

MAP Scale: 4

INTRODUCTION

Layer-by-layer 3D printing technologies, i.e., the precise layer-by-layer deposition of materials, such as metals, concrete, ceramics, polymers, or bioinks, find applications in diverse disciplines, including architecture,[1,2] aerospace,[3,4] automotive,[5,6] electronics, consumer products[7-9] and life sciences,[10-13] setting a benchmark for future manufacturing. In biomedical engineering, 3D printing technologies have been utilized to create bioinspired, extracellular matrix-mimicking scaffolds that encapsulate living cells and feature tissue or organ-like properties.[14-21] Among the

[1] Chemical and Biomolecular Engineering, University of California, Los Angeles, Los Angeles, CA 90095, USA
[2] Institute of Functional Interfaces, Karlsruhe Institute of Technology, Hermann-von-Helmholtz-Platz 1, 76344 Eggenstein-Leopoldshafen, Germany
[3] Institute of Organic Chemistry, Karlsruhe Institute of Technology, Fritz-Haber-Weg 6, 76131 Karlsruhe, Germany
[4] California NanoSystems Institute, University of California, Los Angeles, Los Angeles, CA 90095, USA
[5] Institute for Carbon Management, University of California, Los Angeles, Los Angeles, CA 90095, USA
[*] Correspondence: samsri@ucla.edu
[†] Equal contributions

various 3D printing technologies, extrusion-based bioprinting (EBB) has enjoyed considerate attention for bioprinting owing to versatility, low costs, fast manufacturing time, and the ability to print with inks with high cell loadings.[22,23] However, the development of suitable bioinks within the biofabrication window that possess the optimal balance among printability, post-printing shape fidelity, and biological response remains a significant bottleneck hindering the advancement of EBB technologies.[19,24-30]

Gelatin methacryloyl (GelMA)-based bioinks are one of the most popular and well-studied bioinks that finds a satisfactory balance between shape fidelity and bio-response.[31-34] Their broad commercial availability, simple chemical synthesis from gelatin, temperature-tunable viscoelastic properties, outstanding biocompatibility, surface adhesion characteristics for cells, and biodegradability encourage their widespread use as model inks in tissue engineering.[35-38] Yet, gelatin and other naturally derived polymers, which are obtained by extraction from animal tissues, suffer from limited translation to biomedical contexts due to undesired flow properties of their solutions, including liquid-like behavior at 37 °C and weak response to stresses prior to secondary crosslinking as well as batch-to-batch variability in the manufacturing process leading to variation in size, charge, and polydispersity of the polymer chains.[22,39] In comparison, synthetic polymers, especially poly(ethylene glycol) (PEG) derivatives such as PEG dimethacrylate (PEGDMA), do not face such limitations because of their synthetic origin but typically lack biological functionality, suffer from intrinsic protein repellency, and exhibit low viscosities that are below the threshold of practical use in EBB leading to undesirable flows and loss of form following deposition.[14,40,41]

The complementary benefits and shortcomings of gelatin and PEG-based (bio)inks have inspired attempts to combine them into one formulation. Such approaches aimed at utilizing the controlled biological activity of GelMA (such as cell adhesion and enzymatic degradability) with the controlled non-toxic mechanical reinforcements provided by PEG. PEG-GelMA hybrid hydrogels have been discussed extensively but have been limited to formulations where gelatin and PEG building blocks were covalently co-crosslinked to each other.[42-45] Studies wherein one of the networks is formed via physical interactions, providing an independent and mechanical platform and supporting the crosslinking of the other network, are still lacking.

To address this biomaterials technology gap, we recently introduced versatile, biocompatible ink additives based on complex-forming block polyelectrolytes (bPEs), which enhance the printability of liquid-like EBB-inks.[46] Our recently reported strategy of using highly charged PEG macromolecules has been the first demonstration of harnessing electrostatic and spontaneous self-assembly for smart bioink design.[46,47] In our model inks, oppositely charged bPEs were employed as building blocks of electrostatic self-assemblies (micelles or interconnected networks)[48-51] and combined with GelMA, a representative low-viscosity ink lacking printability at 37 °C. Mixing the ink constituents resulted in hybrid GelMA/bPE inks with excellent 3D printing performance. The bPE additives provided protective scaffoldings preventing dilution in water[52] and loss of structural integrity after deposition.[46] In addition, the hybrid GelMA/bPE hydrogels obtained after photocrosslinking exhibited improved robustness owing to the synergic effects of the entanglement of covalent and electrostatic networks.[46]

In this study, we demonstrate the printability of GelMA/bPE inks at temperatures exceeding the typical melting point of gelatin and provide a parametric study of the mechanical properties of the newly developed hybrid inks that are relevant for extrusion-based bioprinting. The self-assembled structures of bPE complexes are argued to ameliorate the mechanical properties of the GelMA-based inks. Variations in bPE, GelMA concentration, and methacrylation levels revealed valuable insights into how the ink constituents influence overall viscoelastic behavior. The analysis presented here provides a detailed understanding of the novel GelMA/bPE inks and fosters further applications in 3D bioprinting and medical injections.

Results and Discussion

GelMA/bPE Inks are Printable at Physiological Temperatures

GelMA solutions, synthesized from porcine skin gelatin sources (**Figure S1** in the Supplementary information), exhibit excellent printability at 22 °C, below their gelling temperature.[13,53] However, at 37 °C, GelMA solutions exhibit a low shear strength[54,55] and are often *unprintable*. This transition is evident in **Figure 1A**, where GelMA inks ($C_{GelMA} = 5$ wt%) exhibited a well-known thermally induced decline in the shear moduli spanning over 3 orders of magnitude (depicted by black squares). The approximate cross-over point between the storage and loss moduli (G' and G'', respectively) at T = 25 °C

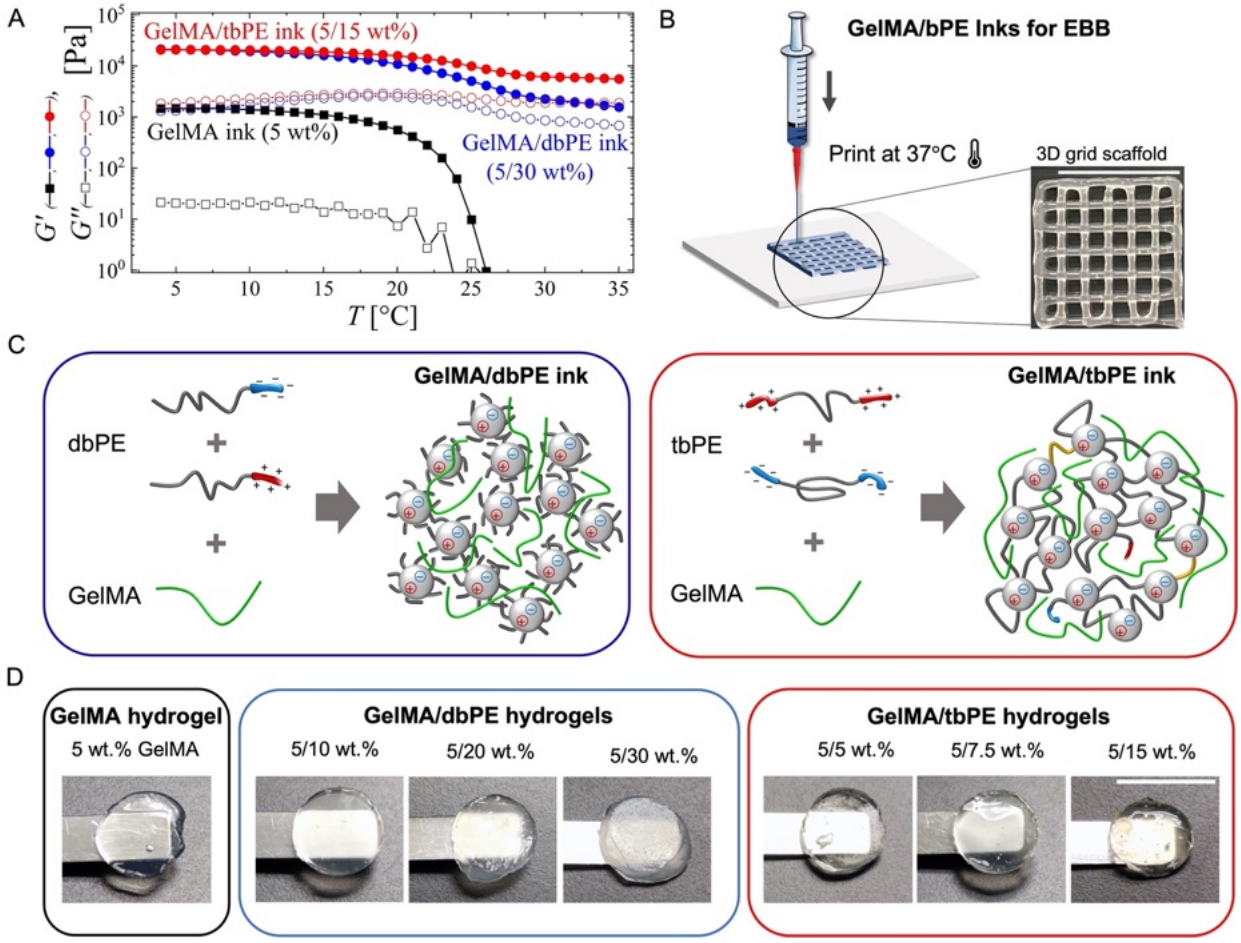

Figure 1: bPE reinforced GelMA inks are 3D printable at physiological temperatures. (A) Temperature evolution of the storage, G', and loss moduli, $G''$of GelMA and GelMA/bPE inks demonstrate the gel-sol transition of GelMA inks while GelMA/bPE inks sustain a high modulus upon heating to physiological temperatures. The moduli were measured with small amplitude oscillatory shear measurements at an angular frequency, $\omega = 1$ rad·s^{-1} and strain, $\gamma = 1\%$. **(B)** A representative example of extrusion printing of GelMA/dbPE inks to a 12 x 12 mm grid structure. Scale bar = 1 cm. **(C)** Schematics representing the microstructure of GelMA/bPE inks comprising bPE self-assemblies with interspersed GelMA chains. Mixing oppositely charged diblock polyelectrolytes (dbPEs) forms polyelectrolyte complex (PEC) micelles while mixing triblock polyelectrolytes (tbPEs) forms of interconnected networks comprising neutral blocks bridging the PEC domains. **(D)** A series of photographs depicting hydrogel compositions obtained after photocrosslinking GelMA and GelMA/bPE inks. Scale bar = 1 cm.

indicates a gel-sol transition. This behavior has been previously reported and has been attributed to the reversible disassembly of hydrogen-bonded triple helices of gelatin chains upon heating.[54]

Pairs of oppositely charged bPE additives imbued 37 °C printability to GelMA solutions by transforming them into self-assembled hydrogels. Previous work has shown that the complexation of oppositely charged bPEs, when restricted at the nanoscale, results in the formation of polyelectrolyte complex (PEC) hydrogels that feature tunability of viscoelastic properties across a broad range and microstructural diversity.[48-50] We utilize these self-assembled hydrogels to provide the initial robustness to the inks, mitigating unwanted flows and enhancing shape fidelity upon deposition prior to photocrosslinking of GelMA chains.

The oppositely charged bPEs we employed comprised poly(ethylene oxide) (PEO) and poly(allyl glycidyl ether) (PAGE) blocks, with the latter functionalized post-synthesis with ionizable groups (guanidinium chloride and sodium sulfonate) to create oppositely charged diblock polyelectrolytes (dbPEs) or triblock polyelectrolytes (tbPEs). The synthesis and characterization of these bPEs are described in **Schemes 1** and **2** and **Figures S2** and **S3** in the Supplementary Information. **Figure 1C** shows a schematic of the improved GelMA/bPE inks comprising uncrosslinked GelMA mixed with either oppositely charged dbPEs or

tbPEs. PEC domains form swiftly upon mixing of the dbPE or the tbPE pairs due to associative phase separation of the charged blocks.[49,50] At sufficiently high polymer concentrations, dbPEs form hydrogels comprising jammed micelles composed of PEC domains and surrounded by neutral PEO coronae, while tbPEs form interconnected networks wherein a significant fraction of the neutral blocks bridge the PEC domains while a small fraction form loops (**Figure 1C**). In this work, these hydrogels will be referred to as dbPE and tbPE inks. In either case, the GelMA chains remain dispersed in the bPE inks, resulting in GelMA/bPE inks. We note that the dbPE and tbPE pairs were functionalized from the same PEO-PAGE and PAGE-PEO-PAGE block copolymers, respectively, and mixed in charge equivalent amounts. Therefore, charge mismatch between the oppositely charged bPEs was eliminated, resulting in strongly segregated PEC domains.

The moduli of the GelMA/bPE inks remained significantly higher than those of the corresponding GelMA inks at temperatures approaching 37 °C (**Figure 1A**). For $T \leq 25$ °C, the GelMA/bPE ink moduli were an order of magnitude higher than those of GelMA inks. Similar to GelMA inks, temperature-induced reductions in the moduli were observed for both GelMA/dbPE and GelMA/tbPE inks, which can again be attributed to the disruption of the hydrogen-bonded GelMA networks. However, the bPE self-assemblies provided sufficient shear strength to the hybrid inks at 37 °C. Furthermore, the GelMA/tbPE inks exhibited higher moduli as compared to the GelMA/dbPE inks, which could be attributed to the robustness of the PEC network present in the former providing larger shear strength in comparison to the jammed micelles in the latter systems. Overall, it can be surmised that the addition of complex-forming bPEs to GelMA can render inks and bioinks, which can be tuned for injection across a range of biologically relevant temperatures.

To demonstrate the extrusion-based printability of the GelMA/bPE inks, 12 × 12 mm grid structures were printed using GelMA/dbPE inks (**Figure 1B**). The structures were printed at 37 °C, which exceeds the melting temperature of gelatin solutions. In the absence of the bPE additives, printing pure GelMA would have led to uncontrolled flows and a complete lack of shape fidelity (**Figure S4**). The grid shape illustrates the structural integrity and stability of the ink during the deposition of multiple layers at 37 °C, serving as a demonstration of overcoming the challenges involved in printing gelatin-based inks at physiological temperatures.

We also demonstrate that the addition of bPEs did not impede the photocrosslinking (photocuring) of the GelMA chains in a series of images in **Figure 1D.** The cured hydrogels remained transparent upon bPE addition, allowing for UV penetration and crosslinking among GelMA chains. The hydrogels, when cured in a cylindrical mold, retained their shape upon extraction from the mold and appeared similar to cured GelMA hydrogels. Scanning electron micrographs (**Figure S5**) depict the microstructure after photocrosslinking and reveal minimal differences between pure GelMA and GelMA/bPE hydrogels.

GelMA/bPE Inks Possess Hierarchical Microstructures

Contemporary hydrogels for tissue engineering applications need to possess mechanical properties commensurate with human tissues and pursue similarities with the tissue microstructures. Human tissues feature anisotropic hierarchal microstructures such as lamellar structure, which allows for directional biological functions aided by alignments of ordered bilayers.[56] However, the majority of traditional hydrogels (e.g., photocrosslinked GelMA) possess isotropic micro and macro-structures and have limited ability to achieve microstructure complexity unique to biological soft tissues.[43] Thus, GelMA hydrogels that feature tunable microstructures can further make them attractive materials to mimic human tissue structural complexity.

Small angle X-ray scattering (SAXS) revealed the microstructure of GelMA/bPE inks, as depicted in **Figure 2** (see also **Figure S6** in the Supplementary Information). In the absence of bPEs, the spectra for GelMA solutions and crosslinked hydrogels resemble characteristic spectra for polymer solutions and crosslinked polymer networks, respectively (**Figure S6** in the Supplementary Information). In the GelMA/bPE inks, the scattering from the PEC domains consisting of highly dense charged blocks of bPEs and high atomic elements (e.g., sulfur and nitrogen) provide a stronger electron contrast than the surrounding environment and therefore dominate the scattering spectra. **Figures 2A and 2B** show a comparison of the one-dimensional intensity $I(q)$ versus wave vector q of the bPE inks (dashed lines), GelMA/bPE inks, and photocrosslinked GelMA/bPE hydrogels (solid and dotted lines, respectively) with increasing concentrations of dbPEs (C_{dbPE}) and tbPEs (C_{tbPE}), respectively. The bPE inks

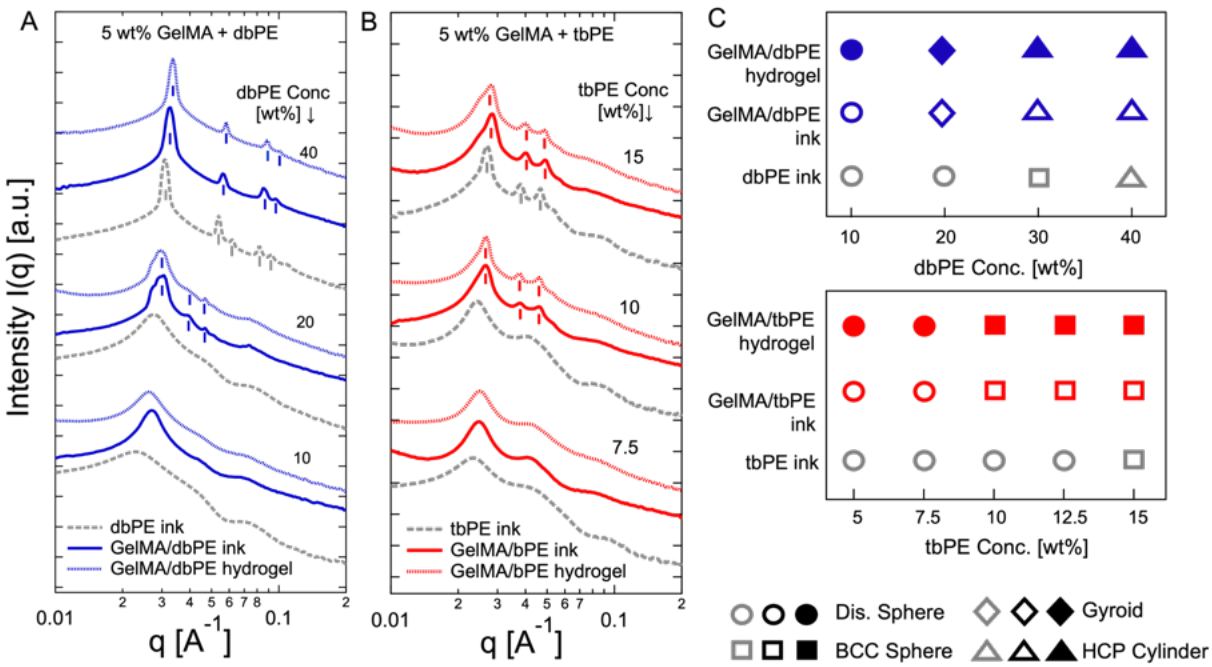

Figure 2: Diverse nanoscale morphologies of GelMA/bPE inks and hydrogels. (A, B) SAXS intensity $I(q)$ versus wave vector q for GelMA/dbPE (A) and GelMA/tbPE (B) inks and hydrogels with varying bPE concentrations. **(C, D)** Morphology maps of GelMA/dbPE (C) and GelMA/tbPE (D) inks and hydrogels with varying bPE concentrations.

(PEC hydrogels) featured a primary peak between q = 0.02 Å^{-1} and 0.03 Å^{-1}, indicating the existence of PEC domains. These primary peaks persisted in both GelMA/dbPE (**Figure 2A**) and GelMA/tbPE (**Figure 2B**) inks and the respective photocrosslinked GelMA/bPE hydrogels, with the peak positioning remaining largely invariant of the presence of GelMA chains in the inks or the interpenetrating network they form upon photocrosslinking.

SAXS spectra with a broad primary peak without any secondary Bragg reflection peaks indicate a disordered arrangement of spherical PEC domains. Such spectra were noted for bPE inks with C_{dbPE} = 10 and 20 wt% (**Figure 2A**) or C_{tbPE} = 5, 7.5, 10, and 12.5 wt% (**Figure 2B**). At higher bPE concentrations, morphological transitions and ordering of PEC domains were observed. For instance, the microstructure of the PEC domains evolved from disordered spheres to ordered spheres (with body-centered cubic arrangements) to hexagonal closely packed (HCP) cylinders in dbPE inks upon increasing C_{dbPE} from 20 wt% to 30 wt% to 40 wt%, respectively (Figure 2C). These transitions were evident from the appearance of the sharp Bragg peaks, as can be noted for 40 wt% dbPE inks in **Figure 2A**, with the secondary peaks being located at $\sqrt{2}q^*$ and $\sqrt{3}q^*$ with respect to the location of the primary peak at q^*, corresponding to BCC arrangements of PEC domains.

Figures 2C and 2D summarize the PEC domain morphology for dbPE and tbPE inks (grey symbols).

Transitions in the morphology of the PEC domains were also noted in response to the combination of GelMA with the bPEs. The presence of 5 wt% GelMA resulted in a transition of the PEC domains from disordered spheres to gyroid or from BCC spheres to HCP cylinders in GelMA/dbPE inks with C_{dbPE} = 20 and 30 wt%, respectively (**Figure 2C**). Similarly, a microstructural transition from disordered spheres to BCC spheres was observed in GelMA/tbPE inks with C_{tbPE} = 10 and 12.5 wt% (**Figure 2D**). In the range of bPE and GelMA concentrations investigated here, microstructural transitions were not noted upon the photocrosslinking of the GelMA/bPE inks; the structures were nearly identical before and after photocrosslinking (solid and dotted lines in **Figures 2A and 2B**).

In contrast, morphological transitions triggered by increasing C_{bPE} in GelMA/bPE inks and hydrogels were attributed to the macromolecular crowding induced by GelMA chains, reconfiguring the PEC domains. Similar transitions have been noted upon the incorporation of other crosslinkable polymers in bPE inks (PEC hydrogels).[52] We further posit that the macromolecular crowding induced by the GelMA chains also results in a lower extent of jamming among the PEC micelles

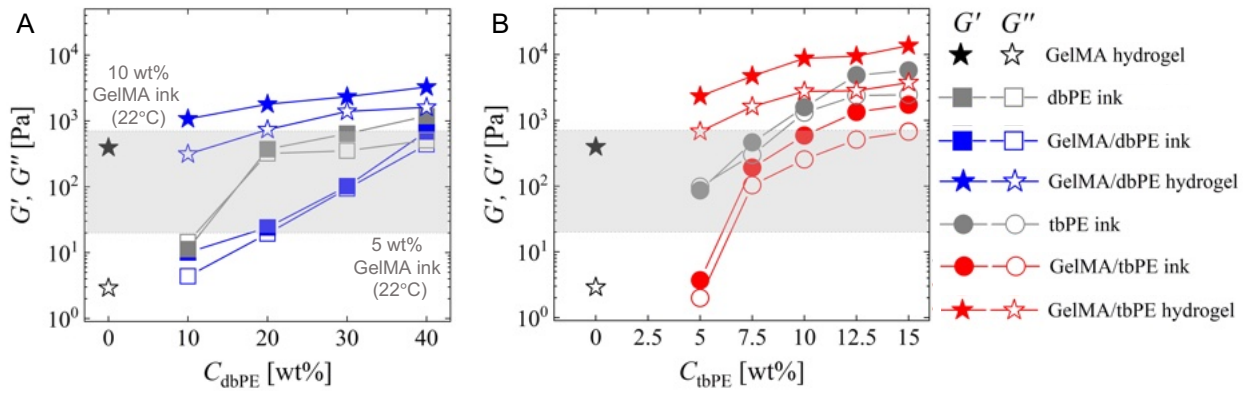

Figure 3: GelMA/bPE ink and hydrogel moduli can be tuned by varying bPE concentrations. (A, B) Storage (G') and loss (G'') moduli of for GelMA/dbPE (A) and GelMA/tbPE (B) inks and hydrogels with varying bPE concentrations C_{bPE}. The moduli were measured with small amplitude oscillatory shear measurements at an angular frequency = 1 rad·s^{-1} and strain = 1% at 37 °C. The shaded region in both (A) and (B) depict the moduli window of fabrication, corresponding to the storage moduli of GelMA inks with concentrations varying between 5 and 10 wt%, measured at 22 °C.

formed by dbPEs (with decreased interdigitation among the micellar coronae) and partial reconfiguration of the PEC network formed by tbPEs (with a larger fraction of midblock chains forming loops as compared to bridging between adjoining PEC domains), respectively. These reconfigurations would not be captured by the scattering spectra but are expected to manifest in the rheological response of the GelMA/bPE inks (discussed in the following sections). More importantly, these scattering investigations reveal that the presence of GelMA chains does not disrupt the self-assembly of the oppositely charged bPE chains. Moreover, as compared to the amorphous structure of pure GelMA hydrogels, the incorporation of bPEs in the GelMA inks and hydrogels enriched its microstructural diversity, broadening the utility of GelMA in tissue engineering applications.

Tunable Linear Viscoelastic Response of GelMA/bPE Inks

Bulk rheological investigations lend themselves as a facile tool to assess the printability and the mechanical integrity of inks prior to and post-printing.[27,57] Therefore, we investigated the viscoelastic response of the bPE and GelMA/bPE inks by imposing small angle oscillatory strain on the inks. Representative response of bPE inks at 37 °C with and without GelMA to oscillatory strain within the linear viscoelastic (LVE) regime is presented in **Figures S7** and **S8** in the Supplementary Information. The storage and loss moduli (G' and G'') of dbPE inks (C_{dbPE} = 20 wt%) were similar across the range of ω investigated here. Moreover, an order of magnitude reduction in both G' and G'' was noted upon the addition of 5 wt% GelMA in the dbPE inks. In contrast, tbPE inks (**Figure S7** and **S8** in the Supplementary Information) exhibited only a minor reduction in the overall magnitude of the LVE response when GelMA was added.

The evolution of the shear moduli of GelMA/dbPE inks as a function of C_{dbPE} is shown in **Figure 3A**. The moduli of GelMA/dbPE inks were generally lower than the corresponding dbPE inks (comparing data sets depicted by squares and circles). The moduli of dbPE inks increased rapidly from C_{dbPE} = 10 to 20 wt%, then plateaued ~ 10^3 Pa at $C_{dbPE} \geq$ 20 wt%. In contrast, both G' and G'' increased almost linearly with increasing C_{dbPE} in GelMA/dbPE inks. A smaller impact of GelMA inclusion on the GelMA/dbPE ink moduli was noted at low C_{dbPE} and could be ascribed to low interdigitation of the micellar coronae. In contrast, at higher C_{dbPE} = 40 wt%, significant interdigitation of micellar coronae can accommodate the GelMA chains without the moduli decreasing markedly. More importantly, G' for the GelMA/dbPE inks with $C_{dbPE} \geq$ 20 wt% all lay within the window of fabrication (corresponding to the G' of 5 wt% and 10 wt% GelMA inks, measured at 22 °C). Therefore, extrusion-based (bio)printing can be accomplished with GelMA/dbPE inks with $C_{dbPE} \geq$ 20 wt%.

The effect of GelMA on the moduli of tbPE inks, in contrast, was most pronounced at the lowest tbPE concentrations, C_{tbPE}= 5 wt% wherein G' and G'' reduced by ~1.5 orders of magnitude (**Figure 3B**). For $C_{tbPE} \geq$ 7.5 wt%, while the shear moduli of GelMA/tbPE inks tended to be lower than the moduli of the tbPE inks,

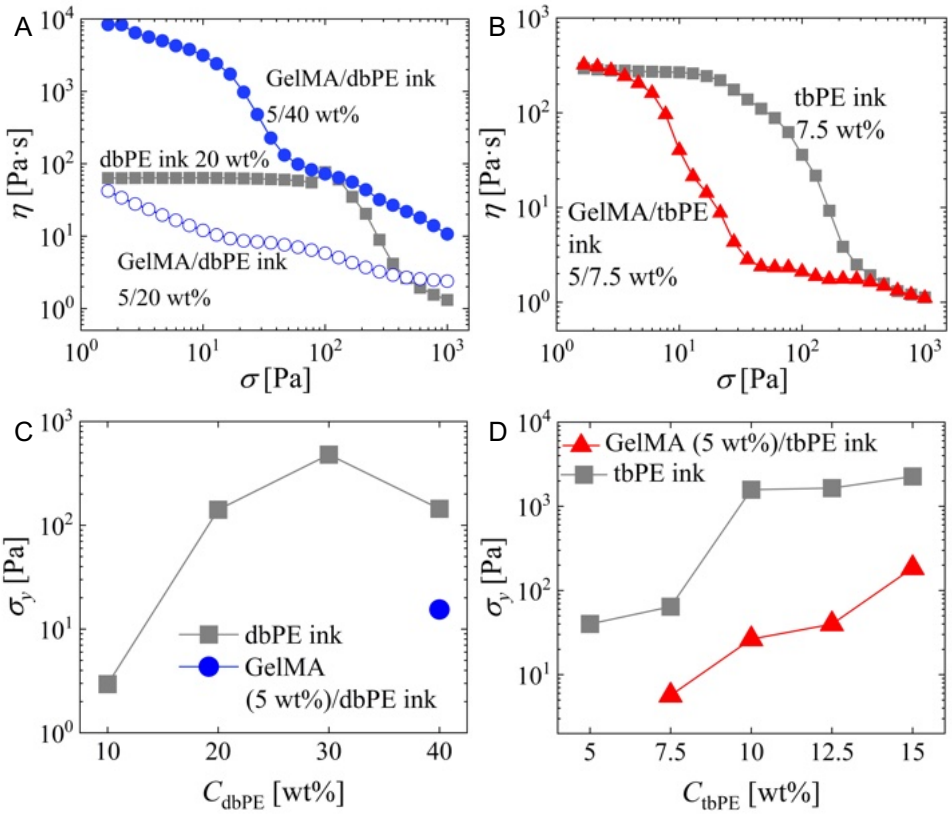

Figure 4: Yielding behavior of GelMA/bPE hybrid inks. (A, B) Shear viscosity, η, as a function of shear stress, σ, for (A) dbPE (C_{dbPE} = 20 wt%) and GelMA/dbPE inks (C_{dbPE} = 20 and 40 wt%, C_{GelMA} = 5 wt%), and (B) tbPE (C_{tbPE} = 7.5 wt%) and GelMA/tbPE inks (C_{tbPE} = 7.5 wt%, C_{GelMA} = 5 wt%). **(C, D)** Yield stress, σ_y, as a function of bPE concentration for (C) dbPE and GelMA/dbPE, and (D) tbPE and GelMA/tbPE inks. All measurements conducted at 37 °C.

they could be considered proximal to each other. With increasing C_{tbPE}, the extent of segregation of the PEC domains is expected to diminish owing to a higher fraction of bridging PEO midblocks, even in the presence of GelMA chains, resulting in the sustenance of the moduli. And, again, G' for the GelMA/tbPE inks with 5 wt% $\leq C_{tbPE} \leq$ 10 wt% lay within the window of fabrication, signifying their utility for extrusion-based (bio)printing.

Photocrosslinking GelMA in the GelMA/bPE inks using ultraviolet (UV) irradiation led to a notable enhancement in the shear moduli. The formation of interlaced water-laden PEC and GelMA networks resulted in GelMA/bPE hydrogels with robust shear moduli. The moduli values of the hydrogels in their crosslinked state were more pronounced at low concentrations where two to three orders of magnitude increase in G' in both GelMA/bPE hydrogels (comparing circles with stars) were noted (**Figures 3A and 3B**, see also **Figure S9** in the Supplementary Information). At higher C_{bPE}, shear moduli of the hydrogels exhibited enhancements of nearly an order of magnitude when compared to their moduli in their ink state.

GelMA/bPE Inks Exhibit Tunable Yielding and Shear Thinning Characteristics

Well-defined yield stress behavior is a common requirement for bioinks that allows for suspending cells in a syringe, but by applying sufficient stress, a flow initiation point can be achieved. This is an important consideration because it determines the required pressure for extrusion.[58] We quantify the yield stress behavior (the stress required for the materials to flow or yielding transition, $\sigma \gtrsim \sigma_y$) at 37 °C to further establish the suitability of GelMA/bPE formulations as 3D printing inks. **Figure 4A** depicts a comparison of the viscosity, $\eta = \sigma/\dot{\gamma}$, as a function of shear stress, σ, for dbPE inks with C_{dbPE} = 20 wt% and GelMA/dbPE inks with C_{dbPE} = 20 and 40 wt% and C_{GelMA} = 5 wt% (see also **Figure S10** in the Supplementary Information). In these flow curves, the stress corresponding to the crossover point of η from the solid ($\sigma < \sigma_y$ with η~constant) to the fluid regime ($\sigma > \sigma_y$, where $\sigma = \sigma_y + \dot{\gamma}^n$) was

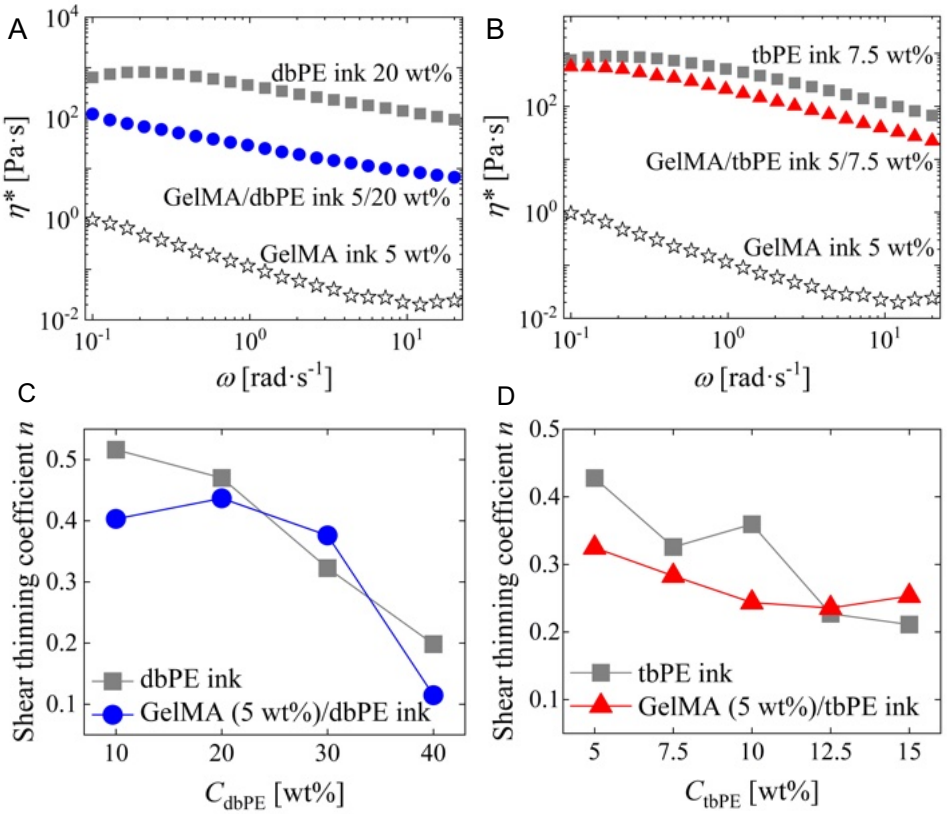

Figure 5: **Shear-thinning behavior of GelMA/bPE inks. (A, B)** Complex shear viscosity, η^*, as a function of angular frequency, ω, for (A) GelMA (C_{GelMA} = 5 wt%), dbPE (C_{dbPE} = 20 wt%), and GelMA/dbPE (C_{GelMA} = 5 wt%, C_{dbPE} = 20 wt%) inks, and (B) GelMA (C_{GelMA} = 5 wt%), tbPE (C_{tbPE} = 7.5 wt%), and GelMA/tbPE (C_{GelMA} = 5 wt%, C_{tbPE} = 7.5 wt%) inks. **(C, D)** Shear thinning coefficients, n, as a function of bPE concentration for (C) dbPE and GelMA/dbPE, and (D) tbPE and GelMA/tbPE inks. All measurements conducted at 37 °C.

designated as the yield stress σ_y.[59] 20 wt% dbPE inks exhibited a yield point at σ_y = 100 Pa, while no apparent yield point was identifiable for the corresponding GelMA/dbPE inks. Increasing C_{dbPE} up to 40 wt%, however, resulted in GelMA/dbPE inks with a well-defined yield point (σ_y = 15.4 Pa). The measurable σ_y values as a function of C_{dbPE} for dbPE inks without or with GelMA are summarized in **Figure 4C**. dbPE inks behaved as yield stress fluids and demonstrated distinct σ_y values across all C_{dbPE}, where σ_y increased with C_{dbPE} until 30 wt% and then decreased for C_{dbPE} = 40 wt%, The latter could be attributed to the morphological transition of the PEC domains from BCC spheres to HCP cylinders. The presence of GelMA obscured the yielding behavior in dbPE inks except at relatively high C_{dbPE} = 40 wt% where a measurable σ_y value was noted, yet nearly an order of magnitude lower than σ_y for the corresponding dbPE inks. These observations correlate well with the reduction of the shear moduli upon the combination of GelMA and dbPEs in GelMA/dbPE inks (**Figures 3A and 3C**), and can again be attributed to the disrupting effect of GelMA chains on the interdigitation of the micellar coronae and diminished extent of jamming, until at sufficiently high C_{dbPE} wherein the micellar coronae remained adequately interdigitated even in the presence of GelMA chains, enabling stress buildup until yielding.

In contrast, the presence of GelMA did not eliminate the yielding behavior in tbPE inks (**Figure 4B**). However, the σ_y reduced upon the combination of GelMA with the tbPEs (for instance, from σ_y = 70 to 7 Pa for C_{tbPE} = 7.5 wt% and C_{GelMA} = 5 wt%), indicating that the solid regime of the material sustained only until smaller imposed stresses. **Figure 4D** depicts the measurable yield stresses σ_y as a function of C_{tbPE} for tbPE inks and GelMA/tbPE inks. tbPE inks exhibited a yielding transition across a wide range of C_{tbPE} regardless of GelMA inclusion (except at the lowest C_{tbPE} = 5 wt%). The yield stress values, σ_y, however, were consistently lower for GelMA/tbPE inks as compared to the corresponding tbPE inks across all C_{tbPE} values, attributable to a lower fraction of bridging midblocks between the PEC domains in the presence of GelMA and consistent with the observations of lower moduli of

GelMA/tbPE inks as compared to tbPE inks (**Figures 3B and 3D**). At the same time, a monotonic increase of σ_y as a function of C_{tbPE} in both formulations is attributed to the increase in PEC network density. These observations are relevant in cases when the injectability and extrudability of (bio)inks need to be precisely controlled for certain injection parameters (e.g., needle radius and length) and process parameters (injection pressure and flow rate).[58]

A prominent shear-thinning response was also noted for the GelMA/bPE inks (**Figure 5,** see also **Figure S11** in the Supplementary Information). Quantifying the shear-thinning behavior is of importance in determining the velocity of (bio)ink extrusion through a small needle and the associated timescales for material collection during deposition. Here, shear-thinning was observed as a decrease in the complex shear viscosity, η^*, as a function of angular frequency, ω, from small amplitude oscillatory shear experiments. For 20 wt% dbPE inks, we observed a Newtonian response (constant η^* for $\omega < 0.2$ rad·s^{-1}) followed by a shear-thinning response for $\omega > 0.2$ rad·s^{-1} (black squares in **Figure 5A**). Similar behavior was also observed for 7.5 wt% tbPE inks (**Figure 5B**). The shear-thinning response was quantified using the Carreau-Yasuda model, which suggests the ω-dependence of η^* as:

$$\eta^*(\omega) = \eta_0^*[1 + (\lambda\omega)^a]^{\frac{n-1}{a}}$$

with η_0^* being the zero shear complex viscosity, λ being the relaxation time, n being the shear-thinning exponent (power law index), and a describing the width of the transition from a Newtonian shear-independent fluid to a power law fluid.[60]

GelMA/bPE inks also exhibited shear thinning behaviors (**Figures 5A and 5B**), albeit with lower η^* and, in some cases, an inaccessible Newtonian flow regime (**Figure 5A**). The shear-thinning behaviors in such cases were described as a power law with a consistency index K as:

$$\eta^*(\omega) = K\omega^{n-1}$$

The shear-thinning exponent n for the dbPE and GelMA/dbPE inks are summarized in **Figure 5C**. A decrease in n, corresponding to stronger shear thinning, was noted with increasing C_{dbPE} for the dbPE inks. In contrast, n remained nearly constant until $C_{dbPE} \leq 30$ wt% and then sharply decreased at $C_{dbPE} = 40$ wt% for GelMA/dbPE inks. This is consistent with the yielding behavior of the GelMA/dbPE inks, wherein up to concentrations $C_{dbPE} \leq 30$ wt%, no yielding was observed owing to diminished jamming among the micelles and, correspondingly, weak shear thinning was observed as micelles rearrange readily in response to the applied stress while at $C_{dbPE} = 40$ wt%, the micellar coronae are sufficiently jammed leading to a yielding behavior and strong shear thinning once yielding has occurred.

GelMA/tbPE inks also exhibited shear thinning behavior consistent with their yielding behavior. Specifically, a lower fraction of bridging midblocks between the PEC domains in the presence of GelMA resulted in stronger shear thinning behaviors as compared to tbPE inks (**Figures 5B and 5D**). Previously reported models to assess the extrusion velocity use the shear thinning exponent as a key parameter. Control over the shear-thinning behavior, as exemplified here for the GelMA/bPE inks, provides opportunities for tuning and expanding the injectability window of these inks in which printability can be accessed over a range of velocities and collection speeds.[58,61]

Rapid Viscoelastic Recovery of GelMA/bPE Inks

After extrusion through a small nozzle, the recovery of inks (transition from liquid-like to solid-like flow behavior) dictates the resolution of printing, shape fidelity, and the construction of precise multi-layered structures.[57] **Figure 6** contrasts the shear viscosity recovery of GelMA/bPE inks at 37 °C with the recovery of GelMA inks at 22 °C. The time-dependent viscosity η was measured during the sequential application of a high shear rate ($\dot{\gamma} = 100$ s^{-1}) for 250 seconds, followed by a low shear rate ($\dot{\gamma} = 0.01$ s^{-1}) for 500 seconds. GelMA inks (22 °C) required long times (≥ 8 minutes) for viscosity recovery, attributable to the slow recovery of the hydrogen-bonded triple helix structure of gelatin chains. In contrast, GelMA/bPE inks (37 °C) exhibited very fast viscosity recovery.

Inks containing dbPEs exhibited near complete recovery with C_{dbPE}-independent recovery timescales, as evident in **Figure 6A**. A minor decay of the low-$\dot{\gamma}$ viscosity was noted for inks with $C_{dbPE} \geq 30$ wt%, indicating slow structural rearrangements of the jammed PEC micelles. At the same time, inks containing lower concentrations of dbPEs (C_{dbPE} = 20 wt%) exhibited a low η but complete recovery associated with the fast structural rearrangements of the partially jammed PEC micelles.

The recovery of GelMA/tbPE inks, especially at $C_{tbPE} \leq$ 10 wt%, comprised a prominent, near-instant first step

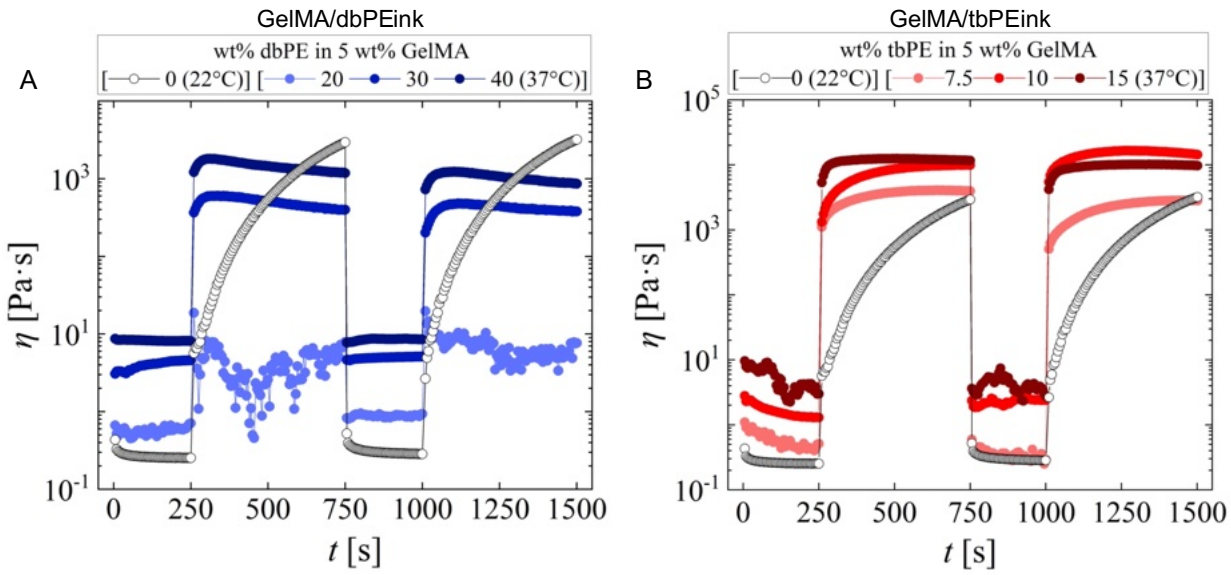

Figure 6: Rapid viscoelastic recovery of GelMA/bPE inks. Swift viscosity recovery after deformation at high shear rates is observed for **(A)** GelMA/dbPE and **(B)** GelMA/tbPE inks at 37 °C. In contrast, GelMA inks recover significantly slowly after shearing at 22 °C. Recovery tests were conducted by applying two sequential steps applying a fixed shear rate, $\dot{\gamma} = 100$ s^{-1} for 250 seconds followed by applying a lower shear rate, $\dot{\gamma} = 0.01$ s^{-1} for 500 seconds. All measurements conducted at 37 °C.

followed by a subtle, slow second step (**Figure 6B**). The slow second step also showed a weak C_{tbPE}-dependence, becoming faster with increasing C_{tbPE}. We attribute this behavior to larger disruption and reconfiguration of the weaker PEC network at low C_{tbPE} owing to low network density. This disruption can also explain the incomplete recovery at low C_{tbPE} transitioning to near complete recovery at high C_{tbPE} (**Figure 6B**). At the same time, the increasing robustness and connectivity of the PEC network led to its larger disruption in the high-$\dot{\gamma}$ regime, resulting in an appreciable thixotropic decrease in η during the first shearing cycle of the high C_{tbPE} inks (**Figure 6B**). We note that thixotropy is a time-dependent decline in viscosity in response to shear stress at a fixed shear rate and is distinguishable from shear-thinning behavior wherein viscosity depends on $\dot{\gamma}$ but is independent of time.[62]

Moduli of GelMA/bPE Inks and Hydrogels can be Modulated by Tuning the Photocrosslinking Density

GelMA-based inks (including the GelMA/bPE inks) are photocurable, demonstrating appropriate stiffness for tissue engineering applications.[43,44,55] We further investigated the effects of GelMA photocrosslinking density, modulated by either its concentration or its methacrylation levels (also referred to as the degree of functionalization, DoF), on the viscoelastic properties of GelMA/bPE inks before and after photocrosslinking. Increasing C_{GelMA} corresponds to a larger number density of GelMA chains and the photocrosslinkable methacrylate groups, whereas increasing DoF corresponds to inks with the same concentration of GelMA chains but with a higher number density of methacrylate groups per GelMA chain.

Generally, the shear moduli were reduced upon increasing C_{GelMA} in GelMA/bPE inks (**Figures 7A and 7B,** see also **Figure S12** and **S13** in the Supplementary Information). The moduli of GelMA/dbPE inks decreased by nearly two orders of magnitude upon increasing C_{GelMA} from 0 to 5 wt%, beyond which they remained nearly constant (**Figure 7A**). In contrast, the moduli of GelMA/tbPE inks weakened monotonically with increasing C_{GelMA}. Consistent with earlier observations, these decay in shear moduli upon increasing GelMA content can be attributed to an increasing reduction of the coronal interdigitations and disruption of the PEC network in the dbPE and tbPE inks by the GelMA chains.

Photocrosslinking GelMA chains in the GelMA/bPE inks led to an opposite trend in moduli evolution. A monotonic increase in the shear moduli, spanning more than an order of magnitude, was noted in both GelMA/dbPE and GelMA/tbPE hydrogels with increasing C_{GelMA} (**Figure 7A and 7B**, star symbols). Elastic moduli were appreciably higher than loss moduli, especially at higher C_{GelMA} values. These moduli enhancements were expected to emerge from

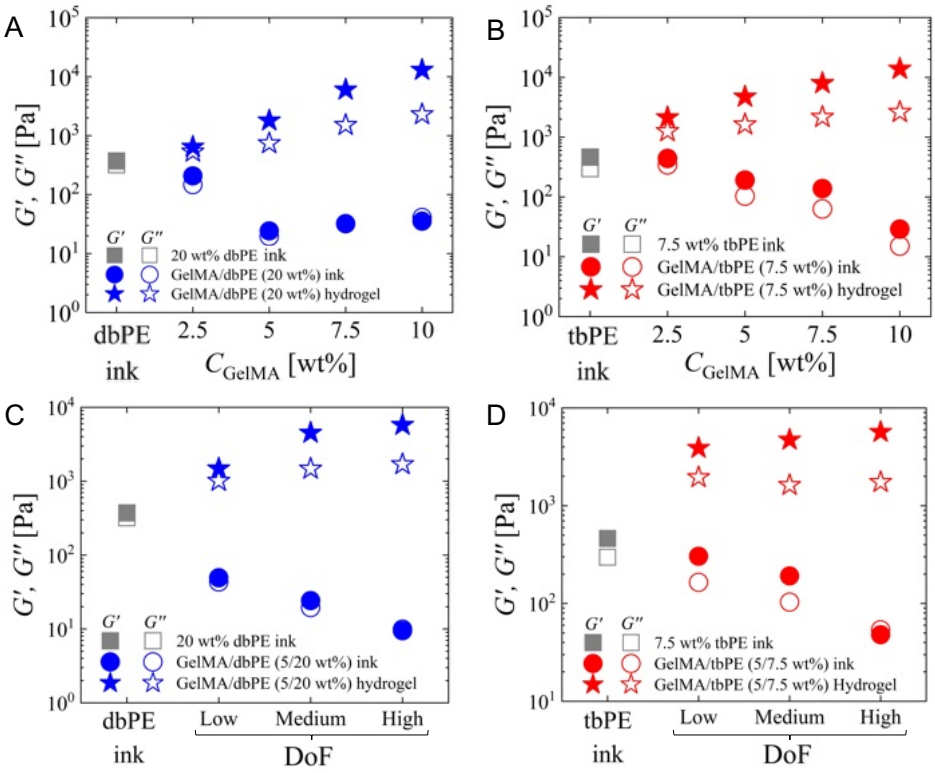

Figure 7: Tunability of ink and hydrogel shear moduli with varying photocrosslinking density. (A, B) Storage (G') and loss (G'') moduli of (A) GelMA/dbPE inks and hydrogels, and (B) GelMA/tbPE inks and hydrogels as a function of GelMA concentration. **(C, D)** The dependence of G' and G'' of (C) GelMA/dbPE inks and hydrogels, and (D) GelMA/tbPE inks and hydrogels on the degree of methacrylate group functionalization or degree of functionalization (DoF) of the GelMA chains. The moduli were measured with small amplitude oscillatory shear measurements at an angular frequency = 1 rad·s^{-1} and strain = 1% at 37 °C.

the higher crosslinking density in the GelMA network and can serve as a guide for tuning the strength of GelMA hydrogels for various tissue engineering purposes.[37]

The level of methacrylate groups, or DoF, along the GelMA chain can be conveniently tuned by controlling the amine substitution with varying amounts of methacrylic anhydride.[54] Previously, higher DoF has been shown to hinder the formation of triple helices between gelatin chains at low temperatures, leading to weaker gels prior to crosslinking.[54] This weakening has been attributed to the hindering of the triple helices formation by the vinyl side groups. The trends of GelMA/bPE ink moduli with increasing GelMA DoF are shown in **Figures 7C and 7D** and are noted to mirror the trends produced upon increasing C_{GelMA}. Increasing the density of vinyl side groups in GelMA led to an observable decrease in G' and G'' owing to increasing hydrophobicity of the GelMA chains resulting in a larger steric hindrance of PEC network.[47] At the same time, photocrosslinking the three GelMA/bPE inks with increasing DoF resulted in progressively increasing stiffness, owing to denser covalent networks and larger interpenetration among the covalent and electrostatic micelles/networks (**Figures 7C** and **7D,** see also **Figure S14 and S15** in the Supplementary Information). Moreover, the increased crosslinking density of the GelMA network can possibly increase jamming among the dbPE micelles by restricting their translational relaxation, and creating additional entanglements with the tbPE networks, resulting in higher hydrogel moduli.

Printability of GelMA/bPE Inks

For extrusion printing, inks are typically inserted into disposable syringes and dispensed either pneumatically or mechanically.[23] In both cases, the printability can be quantified using property-function relationships in which the pressure required to print and the extrusion velocity are the primary control parameters. The changes in viscoelastic properties of inks are expected to result in variation in printability at comparable pressures and extrusion velocities. To test this, we utilized the rheological parameters to assess the printability of GelMA/bPE inks by varying the bPE

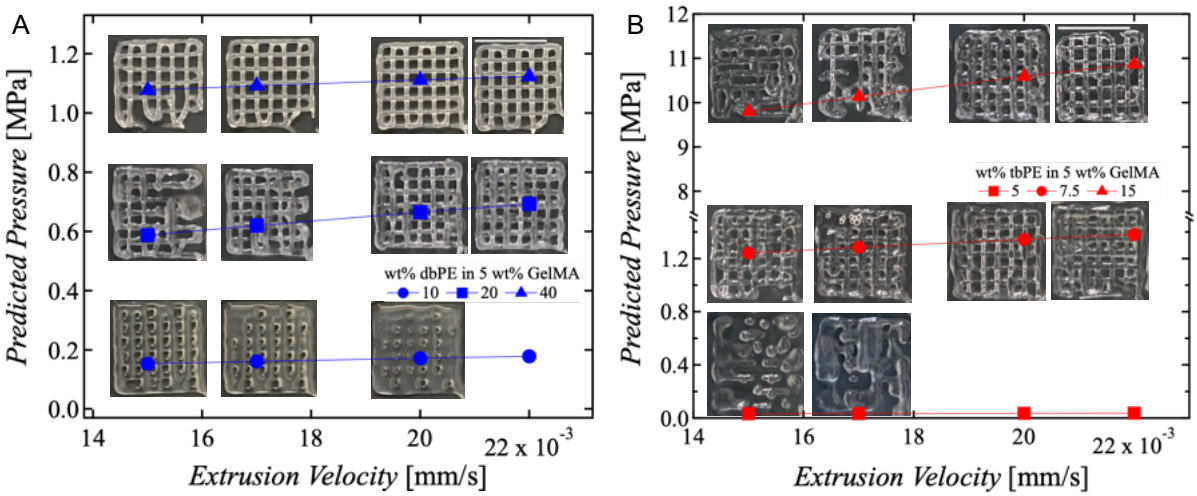

Figure 8: Printability maps of GelMA/bPE inks. Printability of **(A)** GelMA/dbPE and (B) GelMA/tbPE inks as a function of with extrusion pressure and velocity. In these inks, C_{dbPE} was varied between 10 and 40 wt% while C_{tbPE} was varied between 5 and 15 wt%; C_{GelMA} was kept fixed at 5 wt%. Shape fidelity of the printed structures, printed at 37 °C, improved with increasing bPE concentrations, at the expense of higher pressure required for extrusion. Printing demonstrations were made over a range of extrusion velocities ranging from 0.015 to 0.022 mm/s using a needle with radius R = 0.125 mm and length L =32 mm. Scale bars = 1 cm.

concentrations while maintaining a fixed GelMA concentration. A 3D bioprinter (BioSpot BP, Biofluidix GmbH) that extrudes inks using mechanical piston was used to print 12 × 12 mm grid structures at various extrusion speeds, v ranging from 0.015 to 0.022 mm/s. Following previous approaches, we estimate the pressure required for extrusion through a needle (radius, R and length, L) by utilizing parameters obtained from the shear rate-dependent viscosity as:[58,63]

$$P = \left(\frac{3n+1}{n}\right)^n K \left(\frac{Q}{\pi}\right)^n \frac{2L}{R^{3n+1}}$$

The parameters are listed in **Table S1** in the Supplementary Information. We note that (i) the flowrate $Q = \pi R^2 v$ is varied by changing the extrusion velocity in the present study, and (ii) the shear-thinning index n and consistency index K used here were obtained from fitting the shear-thinning regions of the shear rate-dependent viscosity profiles with a power law.

Figure 8 depicts the printability windows of GelMA/bPE inks. Low printing resolution was observed at low C_{bPE} in both GelMA/dbPE (**Figure 8A**) and GelMA/tbPE (**Figure 8B**) inks, attributable to the mechanically weak self-assembled structures formed by the bPEs. The resolution improved at higher concentrations C_{bPE}; the highest resolution was obtained with inks containing C_{dbPE} = 40 wt% and C_{tbPE} =15 wt% in **Figures 8A** and **8B**, respectively. However, with higher bPE concentrations, the predicted pressure required for extrusion also increased as the inks became more robust mechanically and possessed a higher yield stress. We note, however, that the predicted pressures for printability of the GelMA/bPE inks lie within the extrusion pressure range accessible in typical 3D bioprinters.[64] For both the ink systems, optimal printing velocity was observed at v = 0.02 mm/s. At these printing parameters, the GelMA/bPE inks exhibit velocity profile and viscosity recovery that result deposition of inks with minimal merging, breakdown, or spreading of layered structures.

Conclusions

In this contribution, we have demonstrated block polyelectrolyte (bPE) additives that enable 3D printing of gelatin-based inks at physiologically relevant temperatures. The oppositely charged diblock or triblock polyelectrolytes self-assemble to form PEC micelles or three-dimensional networks, respectively. When combined with methacrylated gelatin (GelMA), the bPEs preserved their self-assembly characteristics and hierarchical microstructures. These assemblies served as a scaffolding for the GelMA chains, providing sufficient viscoelastic strength, yielding, and shear thinning characteristics to the GelMA/bPE inks to enable their high fidelity printing at physiological temperatures. In contrast, GelMA solutions, which exhibit a gel-sol transition at temperatures < 30 °C, are unprintable at 37 °C. Moreover, the GelMA/bPE inks

recover significantly faster after shearing (at 37 °C) as compared GelMA inks (at 22 °C), further contributing to the fidelity of the printed structures upon extrusion and deposition. UV irradiation of GelMA/bPE inks resulted in hydrogels composed of interpenetrating electrostatically crosslinked and covalently crosslinked networks.

The microstructure and the viscoelastic properties of the GelMA/bPE inks and hydrogels were facilely tunable by varying the bPE architecture (di- vs. triblock) and concentrations. Moreover, varying the GelMA concentration or degree of functionalization of the methacrylate groups enabled further tunability of the viscoelastic properties of the GelMA/bPE inks both before and after photocrosslinking. By relying on the viscoelastic properties of the inks, we demonstrate an optimal printing window at 37 °C for the GelMA/bPE inks within which the extrusion pressure and velocity are tuned to obtain excellent printing performance and fidelity of the printed structures. We envision that our findings will serve as a practical guide for the bioprinting community to formulate highly customizable extrusion-based inks and encourage the adoption of our additive-based approach to other low-viscosity biomaterials to meet the growing demands of suitable bioinks in EBB and tissue engineering.

MATERIALS AND METHODS

Materials

Potassium (99.5% trace metals basis), naphthalene, poly(ethylene glycol) (Mn = 20,000 g mol-1), poly(ethylene glycol) monomethyl ether (Mn = 5,000 g mol-1), allyl glycidyl ether (AGE), calcium hydride, sodium 3-mercapto-1-propanesulfonate (technical grade, 90%), 1H-pyrazole-1-carboxamidine hydrochloride (99%), cysteamine hydrochloride (≥ 98%), gelatin (type A, gel strength ~300 g bloom, from porcine skin), methacrylic anhydride, 2,2-dimethoxy-2-phenylacetophenone (DMPA) and Irgacure 2959 were purchased from Sigma-Aldrich. Tetrahydrofuran (THF) and dimethylformamide (DMF) were obtained from Fisher Scientific. Dialysis tubes were received from VWR International and Fisher Scientific. DPBS−/− was purchased from Thermo Fisher Scientific.

Synthesis of Gelatin Methacryloyl

Synthesis and purification of gelatin methacryloyl (GelMA) were performed as previously described.[37,65] 10 g gelatin (type A, gel strength ~300 g bloom, from porcine skin, 0.266 mmol NH_2 groups, 1 eq.) was dissolved in 100 mL DPBS. The solution was heated to 50 °C until complete dissolution of gelatin. Then, 3.17 mL methacrylic anhydride (2.13 mmol, 8 eq. per NH_2 group in gelatin) was added dropwise, and the mixture was stirred at 50 °C for 2 h. After dilution with 100 mL DPBS, the solution was transferred into dialysis tubes (molecular weight cutoff; MWCO = 12-14 kDa) and dialyzed against deionized water at 40 °C for 12 cycles of 8 h each. After lyophilization, the product was obtained as a white solid and stored at −20 °C. GelMA with different degrees of functionalization (low, medium, or high) was obtained by varying the amount of methacrylic anhydride (1 eq., 8 eq., or 20 eq. per NH_2 group in gelatin).

^{1}H NMR (400 MHz, D_2O, 315 K): δ/ppm = 7.60-7.40 ($H_{aromtic}$, gelatin), 5.88 (1H, H_a, vinyl), 5.64 (1H, H_b, vinyl), 5.24-0.99 (gelatin), 3.20 (bs, 2H, NH_2), 2.11 (s, 3H, CH_3, H_c) (**Figure S2**, Supplementary Information*).*

Synthesis Triblock Polyelectrolytes

Synthesis, functionalization, and purification of triblock polyelectrolytes were carried out following previously published protocols (**Scheme 2** in the Supplementary Information).[48] Poly(ethylene glycol) (PEO, 20,000 g·mol^{-1}) was dried in a vacuum oven at 25 °C for one day before use. Allyl glycidyl ether (AGE) was mixed with calcium hydride, stirred overnight to remove trace amounts of water, and degassed by three cycles of freeze-pump-thaw, followed by distillation. For copolymer synthesis, all anhydrous reagents were transferred into a glove box under an argon atmosphere. 30 g of PEO was dissolved in 70 mL anhydrous THF at 45 °C and titrated with potassium naphthalenide (0.4 M in anhydrous THF) until the solution turned light green. Then, an appropriate amount (~ 17 mL) of AGE was added, and the reaction mixture was stirred at 45 °C for 48 h. The anionic polymerization was terminated by adding 10 mL degassed methanol. After precipitation in hexane, the product was filtered, and then dried under vacuum prior to further functionalization. The degree of polymerization (DP) of the PAGE blocks was calculated from the relative peak intensities in the NMR spectra, yielding $PAGE_{30}$-PEO_{455}-$PAGE_{30}$.

For subsequent thiol-ene click functionalization, $PAGE_{30}$-PEO_{455}-$PAGE_{30}$, photoinitiator 2,2-dimethoxy-2-phenylacetophenone (DMPA) and a functional thiol reagent (cysteamine hydrochloride or sodium 3-mercapto-1-propanesulfonate, 5 eq. per alkene group) were dissolved in a DMF/water (volumetric ratio of 1:1)

mixture. After degassing with nitrogen for 30 mins, the solutions were irradiated with UV light (365 nm, 8 W) overnight. Then, the product solutions of functionalized copolymers with either ammonium or sulfonate moieties were dialyzed (MWCO = 3.5 kDa) against deionized water for 14 cycles of 8 h each, followed by lyophilization.

Guanidinilated $PAGE_{30}$-PEO_{455}-$PAGE_{30}$ was synthesized from the ammonium functionalized copolymer. An appropriate amount of the ammonium-functionalized tbPE and 1H-pyrazole-1-carboxamidine (4 eq. per ammonium group) was dissolved in 200 mL phosphate-buffered saline (PBS) solution and pH was adjusted to 10 with NaOH. The mixture solution was maintained at pH=10 and stirred for 3 days at room temperature. Then, the product solution was dialyzed (MWCO: 3.5 kDa) against deionized water for 14 cycles of 8 h each, followed by lyophilization. ^{1}H NMR spectra of triblock copolymers prior and after functionalization are provided in **Figure S3** in the Supplementary Information.

Synthesis of Diblock Polyelectrolytes

Synthesis, functionalization, and purification of diblock polyelectrolytes were performed following the same protocol used for the triblock polyelectrolytes, except for replacing the initiator PEO by poly(ethylene glycol) monomethyl ether (mPEG; 5,000 g·mol^{-1}). The DP of the PAGE block was calculated from the relative peak intensities in the NMR spectra, yielding $mPEO_{113}$-$PAGE_{45}$. ^{1}H NMR spectra of diblock copolymers prior to and after functionalization are provided in **Scheme 1 and Figure S2** in the Supplementary Information.

Preparation of GelMA/bPE Inks and Hydrogels

Stock solutions of the block polyanion (sulfonate functionalized dbPE or tbPE), block polycation (guanidinium functionalized dbPE or tbPE), GelMA precursor, and photoinitiator Irgacure 2959 were prepared in DBPS. GelMA/dbPE and GelMA/tbPE inks were obtained by mixing the block polyanion with an aqueous solution of GelMA precursor and photoinitiator, followed by the addition of the block polycation. The molar charge ratio of cationic and anionic moieties of ink was set to 1:1. Each addition step was followed by thorough mixing to ensure homogeneity of the samples. Hydrogels were prepared by exposing the inks to UV light (302 nm, 8 W) for photocrosslinking for 5 minutes.

Small Angle X-Ray Scattering Measurements

Small-angle X-ray scattering (SAXS) measurements were performed at beamline 12-ID-B at the Advanced Photon Source, Argonne National Laboratory. The sample-to-detector distance was set to 4 m, corresponding to a wave vector (q) range of 0.0002 to 0.5 Å^{-1}. bPE and GelMA/bPE inks were loaded into holes (diameter: 3 mm) in 4 mm thick aluminum strips using a positive displacement pipette and sealed on both sides with Kapton tape to avoid water evaporation. Photocrosslinked GelMA/bPE hydrogels were prepared by loading the corresponding inks in the aluminum strips, followed by 5 minutes of UV exposure, and sealing by Kapton tape. All the samples were prepared and loaded onto the sample holders at least 24 h before the SAXS measurements. The samples were exposed to 13 keV X-rays for 0.1 s. All experiments were performed at room temperature. The two- dimensional scattering data were converted into one-dimensional data (I_{sample}) by using the matSAXS package. Sample scattering intensity was acquired by subtracting the appropriately scaled background (solvent) scattering intensity ($I_{solvent}$) from the measured scattering intensity, $I(q) = I_{sample} - \alpha I_{solvent}$, with α being the scaling parameter.

Rheology

Shear rheology measurements were performed on an Anton Paar MCR 302 rheometer. A cone and plate (diameter: 10 mm with a cone angle of 2°) was used for the inks, and a plate-plate geometry (diameter: 8 mm and gap size: 0.6 mm) was used to measure the hydrogels after photocrosslinking. Appropriate amounts of GelMA/bPE inks were loaded on the lower plate and excess volume was trimmed once the cone and plate reach the measuring gap. GelMA/bPE hydrogels were prepared by pipetting 75 μL of ink into a cylindrical polydimethylsiloxane (PDMS) mold (diameter: 8 mm, height: 1.5 mm) and the ink was irradiated with UV radiation for 5 minutes (302 nm, 8 W). The crosslinked GelMA/bPE hydrogels were then transferred into the parallel plate geometry for measuring. Rheological data was acquired at 37 °C for bPE and GelMA-bPE formulations and hydrogels. A solvent trap and a Peltier temperature control system were used to minimize water evaporation and perform temperature ramp experiments. Prior to studying rheological properties, samples were pre-sheared and equilibrated by applying an oscillatory shear γ = 100% for 30 s, followed γ = 1% for 5 mins.

3D Printing Demonstrations

For extrusion-based 3D printing of GelMA/dbPE or GelMA/tbPE inks, the formulations were prepared and filled into a 2 ml syringe (Inkjet Luer Lock Solo, VWR) which was fitted with a conical needle (diameter: 0.25 mm, Vieweg GmbH). The ink-loaded syringe was inserted into a temperature-controlled and piston-driven 3D printer (BioSpot BP, Biofluidix GmbH). The temperature was fixed at 37 °C for 30 min before extrusion. Grid structures were printed (12 × 12 mm) using custom-written G-codes, and photocured under ultraviolet (UV) light for 60 s. The printing speed was set at 5 mm/s during the printing procedure.

Acknowledgments

Research at UCLA was supported by the National Science Foundation (NSF) via the CAREER program (DMR-2048285). Research at the Karlsruhe Institute of Technology (KIT) was funded by the Deutsche Forschungsgemeinschaft (DFG, German Research Foundation) under Germany´s Excellence Strategy via the Excellence Cluster 3D Matter Made to Order (EXC-2082/1 – 390761711). T.G. acknowledges support from the Helmholtz Program Information: Materials Systems Engineering. F.A. acknowledges the funding support of the United Arab Emirates University (UAEU) under the national teaching assistant (TA) program. A.G. acknowledges the funding support by the Karlsruhe House of Young Scientists (KHYS).

Authors contribution

S.S., T.G., and U.S. conceived the study. F.A., T.G., and D.L. performed the synthesis, scattering, and rheology experiments. A.G. and F.M. performed the 3D printing studies. F.A., T.G., and D.L. analyzed and compiled the results. S.S., U.S., T. G., and F.A. edited the manuscript with inputs from D. L. and A.G.

Declaration of Interests

The authors declare no competing interests.

Data statement

All the data reported in this manuscript are available upon request from the corresponding author.

References

1. García-Alvarado, R., Moroni-Orellana, G., and Banda-Pérez, P. (2021). Architectural Evaluation of 3D-Printed Buildings. Buildings *11*, 254. https://doi.org/10.3390/buildings11060254.
2. Sakin, M., and Kiroglu, Y.C. (2017). 3D Printing of Buildings: Construction of the Sustainable Houses of the Future by BIM. Energy Procedia *134*, 702-711. https://doi.org/10.1016/j.egypro.2017.09.562.
3. Nickels, L. (2015). AM and aerospace: an ideal combination. Metal Powder Report *70*, 300-303. https://doi.org/10.1016/j.mprp.2015.06.005.
4. Kumar, L.J., and Krishnadas Nair, C. (2017). Current trends of additive manufacturing in the aerospace industry. Advances in 3D printing & additive manufacturing technologies, 39-54. https://doi.org/10.1007/978-981-10-0812-2_4.
5. Nichols, M.R. (2019). How does the automotive industry benefit from 3D metal printing? Metal Powder Report *74*, 257-258. https://doi.org/10.1016/j.mprp.2019.07.002.
6. Böckin, D., and Tillman, A.-M. (2019). Environmental assessment of additive manufacturing in the automotive industry. Journal of Cleaner Production *226*, 977-987. https://doi.org/10.1016/j.jclepro.2019.04.086.
7. Halassi, S., Semeijn, J., and Kiratli, N. (2019). From consumer to prosumer: a supply chain revolution in 3D printing. International Journal of Physical Distribution & Logistics Management *49*, 200-216. https://doi.org/10.1108/IJPDLM-03-2018-0139.
8. Yoo, B., Ko, H., and Chun, S. (2016). Prosumption perspectives on additive manufacturing: reconfiguration of consumer products with 3D printing. Rapid Prototyping Journal *22*, 691-705. https://doi.org/10.1108/RPJ-01-2015-0004.
9. Gebler, M., Schoot Uiterkamp, A.J.M., and Visser, C. (2014). A global sustainability perspective on 3D printing technologies. Energy Policy *74*, 158-167. https://doi.org/10.1016/j.enpol.2014.08.033.
10. Ozbolat, I.T., Peng, W., and Ozbolat, V. (2016). Application areas of 3D bioprinting. Drug Discovery Today *21*, 1257-1271. https://doi.org/10.1016/j.drudis.2016.04.006.
11. Ozbolat, I.T., and Yu, Y. (2013). Bioprinting Toward Organ Fabrication: Challenges and Future Trends. IEEE Transactions on Biomedical Engineering *60*, 691-699. https://doi.org/10.1109/TBME.2013.2243912.
12. Mironov, V., Kasyanov, V., Drake, C., and Markwald, R.R. (2008). Organ printing: promises and challenges. https://doi.org/10.2217/17460751.3.1.93.
13. Kolesky, D.B., Truby, R.L., Gladman, A.S., Busbee, T.A., Homan, K.A., and Lewis, J.A. (2014). 3D bioprinting of vascularized, heterogeneous cell-laden tissue constructs. Advanced Materials *26*, 3124-3130. https://doi.org/10.1002/adma.201305506.
14. Hospodiuk, M., Dey, M., Sosnoski, D., and Ozbolat, I.T. (2017). The bioink: A comprehensive review on bioprintable materials. Biotechnol Adv *35*, 217-239. https://doi.org/10.1016/j.biotechadv.2016.12.006.
15. Gungor-Ozkerim, P.S., Inci, I., Zhang, Y.S., Khademhosseini, A., and Dokmeci, M.R. (2018).

Bioinks for 3D bioprinting: an overview. Biomaterials Science *6*, 915-946. https://doi.org/10.1039/C7BM00765E.
16. Bishop, E.S., Mostafa, S., Pakvasa, M., Luu, H.H., Lee, M.J., Wolf, J.M., Ameer, G.A., He, T.-C., and Reid, R.R. (2017). 3-D bioprinting technologies in tissue engineering and regenerative medicine: Current and future trends. Genes & Diseases *4*, 185-195. https://doi.org/10.1016/j.gendis.2017.10.002.
17. Valot, L., Martinez, J., Mehdi, A., and Subra, G. (2019). Chemical insights into bioinks for 3D printing. Chemical Society Reviews *48*, 4049-4086. https://doi.org/10.1039/C7CS00718C.
18. Moroni, L., Burdick, J.A., Highley, C., Lee, S.J., Morimoto, Y., Takeuchi, S., and Yoo, J.J. (2018). Biofabrication strategies for 3D in vitro models and regenerative medicine. Nature Reviews Materials *3*, 21-37. https://doi.org/10.1038/s41578-018-0006-y.
19. Sun, W., Starly, B., Daly, A.C., Burdick, J.A., Groll, J., Skeldon, G., Shu, W., Sakai, Y., Shinohara, M., Nishikawa, M., et al. (2020). The bioprinting roadmap. Biofabrication *12*, 022002. https://doi.org/10.1088/1758-5090/ab5158.
20. Murphy, S.V., and Atala, A. (2014). 3D bioprinting of tissues and organs. Nature Biotechnology *32*, 773-785. https://doi.org/10.1038/nbt.2958.
21. Arslan-Yildiz, A., Assal, R.E., Chen, P., Guven, S., Inci, F., and Demirci, U. (2016). Towards artificial tissue models: past, present, and future of 3D bioprinting. Biofabrication *8*, 014103. https://doi.org/10.1088/1758-5090/8/1/014103.
22. Bedell, M.L., Navara, A.M., Du, Y., Zhang, S., and Mikos, A.G. (2020). Polymeric Systems for Bioprinting. Chemical Reviews *120*, 10744-10792. https://doi.org/10.1021/acs.chemrev.9b00834.
23. Ozbolat, I.T., and Hospodiuk, M. (2016). Current advances and future perspectives in extrusion-based bioprinting. Biomaterials *76*, 321-343. https://doi.org/10.1016/j.biomaterials.2015.10.076.
24. Malda, J., Visser, J., Melchels, F.P., Jüngst, T., Hennink, W.E., Dhert, W.J., Groll, J., and Hutmacher, D.W. (2013). 25th anniversary article: engineering hydrogels for biofabrication. Advanced Materials *25*, 5011-5028. https://doi.org/10.1002/adma.201302042.
25. Levato, R., Jungst, T., Scheuring, R.G., Blunk, T., Groll, J., and Malda, J. (2020). From shape to function: the next step in bioprinting. Advanced Materials *32*, 1906423. https://doi.org/10.1002/adma.201906423.
26. Ouyang, L. (2022). Pushing the rheological and mechanical boundaries of extrusion-based 3D bioprinting. Trends in Biotechnology *40*, 891-902. https://doi.org/10.1016/j.tibtech.2022.01.001.
27. Paxton, N., Smolan, W., Böck, T., Melchels, F., Groll, J., and Jungst, T. (2017). Proposal to assess printability of bioinks for extrusion-based bioprinting and evaluation of rheological properties governing bioprintability. Biofabrication *9*, 044107. https://doi.org/10.1088/1758-5090/aa8dd8.
28. Lee, S.C., Gillispie, G., Prim, P., and Lee, S.J. (2020). Physical and Chemical Factors Influencing the Printability of Hydrogel-based Extrusion Bioinks. Chemical Reviews *120*, 10834-10886. https://doi.org/10.1021/acs.chemrev.0c00015.
29. Blaeser, A., Duarte Campos, D.F., Puster, U., Richtering, W., Stevens, M.M., and Fischer, H. (2016). Controlling shear stress in 3D bioprinting is a key factor to balance printing resolution and stem cell integrity. Advanced healthcare materials *5*, 326-333. https://doi.org/10.1002/adhm.201500677.
30. Townsend, J.M., Beck, E.C., Gehrke, S.H., Berkland, C.J., and Detamore, M.S. (2019). Flow behavior prior to crosslinking: The need for precursor rheology for placement of hydrogels in medical applications and for 3D bioprinting. Progress in Polymer Science *91*, 126-140. https://doi.org/10.1016/j.progpolymsci.2019.01.003.
31. Xie, M., Yu, K., Sun, Y., Shao, L., Nie, J., Gao, Q., Qiu, J., Fu, J., Chen, Z., and He, Y. (2019). Protocols of 3D bioprinting of gelatin methacryloyl hydrogel based bioinks. JoVE (Journal of Visualized Experiments), e60545. https://doi.org/10.3791/60545.
32. Nichol, J.W., Koshy, S.T., Bae, H., Hwang, C.M., Yamanlar, S., and Khademhosseini, A. (2010). Cell-laden microengineered gelatin methacrylate hydrogels. Biomaterials *31*, 5536-5544. https://doi.org/10.1016/j.biomaterials.2010.03.064.
33. Gaudet, I.D., and Shreiber, D.I. (2012). Characterization of Methacrylated Type-I Collagen as a Dynamic, Photoactive Hydrogel. Biointerphases *7*. https://doi.org/10.1007/s13758-012-0025-y.
34. Burdick, J.A., Chung, C., Jia, X., Randolph, M.A., and Langer, R. (2005). Controlled Degradation and Mechanical Behavior of Photopolymerized Hyaluronic Acid Networks. Biomacromolecules *6*, 386-391. https://doi.org/10.1021/bm049508a.
35. Liu, W., Heinrich, M.A., Zhou, Y., Akpek, A., Hu, N., Liu, X., Guan, X., Zhong, Z., Jin, X., and Khademhosseini, A. (2017). Extrusion bioprinting of shear-thinning gelatin methacryloyl bioinks. Advanced healthcare materials *6*, 1601451. https://doi.org/10.1002/adhm.201601451.
36. Klotz, B.J., Gawlitta, D., Rosenberg, A.J.W.P., Malda, J., and Melchels, F.P.W. (2016). Gelatin-Methacryloyl Hydrogels: Towards Biofabrication-Based Tissue Repair. Trends in Biotechnology *34*, 394-407. https://doi.org/10.1016/j.tibtech.2016.01.002.
37. Yue, K., Trujillo-de Santiago, G., Alvarez, M.M., Tamayol, A., Annabi, N., and Khademhosseini, A. (2015). Synthesis, properties, and biomedical applications of gelatin methacryloyl (GelMA) hydrogels. Biomaterials *73*, 254-271.

https://doi.org/10.1016/j.biomaterials.2015.08.045.
38. Janmaleki, M., Liu, J., Kamkar, M., Azarmanesh, M., Sundararaj, U., and Nezhad, A.S. (2021). Role of temperature on bio-printability of gelatin methacryloyl bioink in two-step cross-linking strategy for tissue engineering applications. Biomedical Materials *16*, 015021. https://doi.org/10.1088/1748-605X/abbcc9.
39. Pati, F., Jang, J., Lee, J.W., and Cho, D.-W. (2015). Chapter 7 - Extrusion Bioprinting. In Essentials of 3D Biofabrication and Translation, A. Atala, and J.J. Yoo, eds. (Academic Press), pp. 123-152. https://doi.org/10.1016/B978-0-12-800972-7.00007-4.
40. Ashammakhi, N., Ahadian, S., Xu, C., Montazerian, H., Ko, H., Nasiri, R., Barros, N., and Khademhosseini, A. (2019). Bioinks and bioprinting technologies to make heterogeneous and biomimetic tissue constructs. Materials Today Bio *1*, 100008. https://doi.org/10.1016/j.mtbio.2019.100008.
41. Hölzl, K., Lin, S., Tytgat, L., Van Vlierberghe, S., Gu, L., and Ovsianikov, A. (2016). Bioink properties before, during and after 3D bioprinting. Biofabrication *8*, 032002. https://doi.org/10.1088/1758-5090/8/3/032002.
42. Gao, G., Schilling, A.F., Hubbell, K., Yonezawa, T., Truong, D., Hong, Y., Dai, G., and Cui, X. (2015). Improved properties of bone and cartilage tissue from 3D inkjet-bioprinted human mesenchymal stem cells by simultaneous deposition and photocrosslinking in PEG-GelMA. Biotechnology Letters *37*, 2349-2355. https://doi.org/10.1007/s10529-015-1921-2.
43. Hutson, C.B., Nichol, J.W., Aubin, H., Bae, H., Yamanlar, S., Al-Haque, S., Koshy, S.T., and Khademhosseini, A. (2011). Synthesis and characterization of tunable poly (ethylene glycol): gelatin methacrylate composite hydrogels. Tissue Engineering Part A *17*, 1713-1723. https://doi.org/10.1089/ten.tea.2010.0666.
44. Kim, P., Yuan, A., Nam, K.-H., Jiao, A., and Kim, D.-H. (2014). Fabrication of poly (ethylene glycol): gelatin methacrylate composite nanostructures with tunable stiffness and degradation for vascular tissue engineering. Biofabrication *6*, 024112. https://doi.org/10.1088/1758-5082/6/2/024112.
45. Nemeth, C.L., Janebodin, K., Yuan, A.E., Dennis, J.E., Reyes, M., and Kim, D.-H. (2014). Enhanced chondrogenic differentiation of dental pulp stem cells using nanopatterned PEG-GelMA-HA hydrogels. Tissue Engineering Part A *20*, 2817-2829. https://doi.org/10.1089/ten.tea.2013.0614.
46. Gockler, T., Li, D., Grimm, A., Mecklenburg, F., Grün, M., Schepers, U., and Srivastava, S. (2023). Polyelectrolyte Complex Hydrogel Scaffoldings Enable Extrusion-based 3D Bioprinting of Low-Viscosity Bioinks. ChemRxiv. https://doi.org/10.26434/chemrxiv-2023-v2tx2.
47. Li, D., Göckler, T., Schepers, U., and Srivastava, S. (2022). Polyelectrolyte Complex-Covalent Interpenetrating Polymer Network Hydrogels. Macromolecules *55*, 4481-4491. https://doi.org/10.1021/acs.macromol.2c00590.
48. Hunt, J.N., Feldman, K.E., Lynd, N.A., Deek, J., Campos, L.M., Spruell, J.M., Hernandez, B.M., Kramer, E.J., and Hawker, C.J. (2011). Tunable, high modulus hydrogels driven by ionic coacervation. Advanced Materials *23*, 2327-2331. https://doi.org/10.1002/adma.201004230.
49. Srivastava, S., Levi, A.E., Goldfeld, D.J., and Tirrell, M.V. (2020). Structure, morphology, and rheology of polyelectrolyte complex hydrogels formed by self-assembly of oppositely charged triblock polyelectrolytes. Macromolecules *53*, 5763-5774. https://doi.org/10.1021/acs.macromol.0c00847.
50. Srivastava, S., Andreev, M., Levi, A.E., Goldfeld, D.J., Mao, J., Heller, W.T., Prabhu, V.M., De Pablo, J.J., and Tirrell, M.V. (2017). Gel phase formation in dilute triblock copolyelectrolyte complexes. Nature Communications *8*, 1-9. https://doi.org/10.1038/ncomms14131.
51. Lemmers, M., Voets, I.K., Stuart, M.A.C., and van der Gucht, J. (2011). Transient network topology of interconnected polyelectrolyte complex micelles. Soft Matter *7*, 1378-1389. https://doi.org/10.1039/C0SM00767F.
52. Li, D., Ghovvati, M., Annabi, N., and Srivastava, S. (2023). Polyelectrolyte Complex Scaffoldings for Photocrosslinked Hydrogels. Molecular Systems Design & Engineering. https://doi.org/10.1039/D2ME00171C
53. Bertassoni, L.E., Cardoso, J.C., Manoharan, V., Cristino, A.L., Bhise, N.S., Araujo, W.A., Zorlutuna, P., Vrana, N.E., Ghaemmaghami, A.M., Dokmeci, M.R., and Khademhosseini, A. (2014). Direct-write bioprinting of cell-laden methacrylated gelatin hydrogels. Biofabrication *6*, 024105. https://doi.org/10.1088/1758-5082/6/2/024105.
54. Van Den Bulcke, A.I., Bogdanov, B., De Rooze, N., Schacht, E.H., Cornelissen, M., and Berghmans, H. (2000). Structural and rheological properties of methacrylamide modified gelatin hydrogels. Biomacromolecules *1*, 31-38. https://doi.org/10.1021/bm990017d.
55. Gao, G., Schilling, A.F., Hubbell, K., Yonezawa, T., Truong, D., Hong, Y., Dai, G., and Cui, X. (2015). Improved properties of bone and cartilage tissue from 3D inkjet-bioprinted human mesenchymal stem cells by simultaneous deposition and photocrosslinking in PEG-GelMA. Biotechnology Letters *37*, 2349-2355. https://doi.org/10.1007/s10529-015-1921-2.
56. Yue, Y., and Gong, J.P. (2021). Structure and Unique Functions of Anisotropic Hydrogels Comprising Uniaxially Aligned Lamellar Bilayers. Bulletin of the Chemical Society of Japan *94*, 2221-2234. https://doi.org/10.1246/bcsj.20210209.

57. Cooke, M.E., and Rosenzweig, D.H. (2021). The rheology of direct and suspended extrusion bioprinting. APL Bioengineering *5*, 011502. https://doi.org/10.1063/5.0031475.
58. Lopez Hernandez, H., Souza, J.W., and Appel, E.A. (2021). A Quantitative Description for Designing the Extrudability of Shear-Thinning Physical Hydrogels. Macromolecular Bioscience *21*, 2000295. https://doi.org/10.1002/mabi.202000295.
59. Coussot, P. (2014). Yield stress fluid flows: A review of experimental data. Journal of Non-Newtonian Fluid Mechanics *211*, 31-49. https://doi.org/10.1016/j.jnnfm.2014.05.006.
60. Yasuda, K., Armstrong, R., and Cohen, R. (1981). Shear flow properties of concentrated solutions of linear and star branched polystyrenes. Rheologica Acta *20*, 163-178. https://doi.org/10.1007/BF01513059.
61. Jungst, T., Smolan, W., Schacht, K., Scheibel, T., and Groll, J.r. (2016). Strategies and molecular design criteria for 3D printable hydrogels. Chemical Reviews *116*, 1496-1539. https://doi.org/10.1021/acs.chemrev.5b00303.
62. Mewis, J., and Wagner, N.J. (2009). Thixotropy. Advances in Colloid and Interface Science *147*, 214-227. https://doi.org/10.1016/j.cis.2008.09.005.
63. Chilton, R.A., and Stainsby, R. (1998). Pressure loss equations for laminar and turbulent non-Newtonian pipe flow. Journal of Hydraulic Engineering *124*, 522-529. https://doi.org/10.1061/(ASCE)0733-9429(1998)124:5(522).
64. Thakare, K., Wei, X., Jerpseth, L., Bhardwaj, A., Qin, H., and Pei, Z. (2020). Feasible Regions of Bioink Composition, Extrusion Pressure, and Needle Size for Continuous Extrusion-Based Bioprinting. Journal of Manufacturing Science and Engineering *142*. https://doi.org/10.1115/1.4048000.
65. Göckler, T., Haase, S., Kempter, X., Pfister, R., Maciel, B.R., Grimm, A., Molitor, T., Willenbacher, N., and Schepers, U. (2021). Tuning Superfast Curing Thiol-Norbornene-Functionalized Gelatin Hydrogels for 3D Bioprinting. Advanced Healthcare Materials *10*, 2100206. https://doi.org/10.1002/adhm.202100206.